

## Electronic Supporting Information

### **Deciphering Ligand-Controlled Charge Transfer from Metal-Organic Framework to Cadmium Sulfide for Enhanced Photocatalytic Hydrogen Evolution Reaction**

Ajit Kumar Singh,<sup>a</sup> Arpna Jaryal,<sup>b</sup> Sunil Kumar Patel,<sup>c</sup> Deepak Kumar,<sup>a</sup> E. Siva Subramaniam Iyer,<sup>c,\*</sup> Kamalakannan Kailasam,<sup>b,\*</sup> and Arindam Indra<sup>a,\*</sup>

<sup>a</sup> *Department of Chemistry, Indian Institute of Technology (BHU), Varanasi, UP-221005, India.*  
Email: [arindam.chy@iitbhu.ac.in](mailto:arindam.chy@iitbhu.ac.in)

<sup>b</sup> *Advanced Functional Nanomaterials, Institute of Nano Science and Technology (INST), Knowledge City, Sector-81, Manauli, SAS Nagar, 140306 Mohali, Punjab, India.* Email: [kamal@inst.ac.in](mailto:kamal@inst.ac.in)

<sup>c</sup> *School of Chemical and Materials Sciences, Indian Institute of Technology Goa, Ponda, Goa, India.*  
Email: [essiyer@iitgoa.ac.in](mailto:essiyer@iitgoa.ac.in)

## Experimental Section

### Chemicals

Cadmium nitrate hexahydrate (SRL, India, extra pure), thiourea (Merck, India), ethylenediamine (SRL, India), cobalt acetate tetrahydrate (SRL, India, extra pure), potassium hexacyanoferrate (III) (SRL, India), sodium nitroprusside (SRL, India, extra pure), polyvinylpyrrolidone (PVP, K-30) (SRL, India), and sodium dodecyl sulfate (SDS) (SRL, India, extra pure) were purchased and used without further purification.

Fluorine doped tin oxide coated glass slide (FTO, surface resistivity  $\sim 7 \Omega/\text{sq}$ ) was procured from Sigma-Aldrich and cut into pieces of 1 cm x 2 cm.

### Instruments

The crystal structure and the phases of the synthesized photocatalysts were evaluated by powder X-ray diffraction (PXRD). The PXRD was recorded on a Rigaku Smart Lab 9 kW Powder Type X-Ray diffractometer. The Cu-K $_{\alpha}$  ( $\lambda = 1.5418 \text{ \AA}$ ) radiation was used for the PXRD measurements. The PXRD patterns were recorded in the range of  $5^{\circ} < 2\theta < 80^{\circ}$ .

The IR spectra of the synthesized materials were investigated using a Thermo Scientific Nicolet iS5 FTIR spectrometer under attenuated total reflection (ATR) mode. The IR data were recorded in the range of 600-3600  $\text{cm}^{-1}$ .

X-ray photoelectron spectroscopy (XPS) was carried out using a K-Alpha Thermo Fisher Scientific X-ray photoelectron spectrometer. The XPS data were analyzed by using Origin 8.5 software.

The morphology and surface characteristics were investigated by field emission scanning electron microscopy (FESEM) EVO-Scanning Electron Microscope MA15/18, from CARL ZEISS MICROSCOPY LTD. Energy dispersive X-ray (EDX) analysis was carried out on 51N1000 from EDS Oxford Instruments Nanoanalysis.

Transmission electron microscopic (TEM) studies were carried out using Tecnai G2 F30 TWIN from FEI Company from the USA (SEA) PTE, LTD transmission electron microscope.

Femtosecond transient absorption spectroscopy was used to study the different states in CdS and NP-CdS-2. The ultrafast Transient Absorption (TA) experiments were performed on Helios TA setup. The samples were kept in a sealed quartz cuvette with path length of 2 mm. The samples used in the experiments were suspended in ethanol and the optical density (OD) was maintained  $\sim 0.5$  in 2 mm path length. The sample was stirred using a magnetic stirrer. The pump wavelength of 360 nm (100 nJ) was generated from Operasolo OPA. A White light probe was generated by focussing a fraction of amplified output, centered at 800 nm produced from Astrella Amplifier from Coherent USA operating at 1 kHz, on a CaF $_2$  crystal. The absorption difference spectrum was measured with changing the pump-probe time delay and recorded using a CCD detector at each delay. The TA spectra were analysed using Surface Explorer, V.4.2 software.

### Synthesis of cadmium sulfide nanorods<sup>1</sup>

Cd(NO<sub>3</sub>)<sub>2</sub>·6H<sub>2</sub>O (3.11 mmol) and thiourea (9.32 mmol) were dissolved in 15 mL ethylenediamine separately. The thiourea solution was added into cadmium nitrate solution and stirred for 15 minutes. The whole solution was transferred into a Teflon lined autoclave and heated in an oven at 180 °C for 24 h. The yellow color solid was collected by centrifugation (8000 rpm for 5 minutes) and washed with distilled water for four times. Finally, the solid was washed with ethanol and hexane for three times and dried in a hot-air oven at 80° C for 12 h.

### Synthesis of NP-CdS-1

Cobalt acetate tetrahydrate (10 mg) was dissolved in 50 mL H<sub>2</sub>O, PVP (60 mg) was added into the solution and stirred for 15 minutes to get a homogeneous solution A. 100 mg CdS nanorods were dispersed in 50 mL H<sub>2</sub>O by sonication for 10 minutes to get a mixture B. Solution A was added to B keeping in an ice bath while maintaining the temperature at 1-3 °C and stirred for 30 minutes at that temperature to get the mixture C. An ice-cold solution of sodium nitroprusside (11 mg) and SDS (74 mg) in 10 mL water was added to the mixture C. The whole mixture was kept at 1-3 °C and stirred for 30 minutes. The precipitate was collected by centrifugation (8000 rpm for 10 minutes) and washed with distilled water and ethanol. The obtained precipitate was dried in a hot-air oven at 50 °C for 12 h.

**Note:** Maintaining the temperature between 1-3 °C is extremely important for a low loading of cocatalyst CoFe-NP on CdS surface. At a temperature >5 °C, a higher loading of CoFe-NP was observed. High loading of CoFe-NP on CdS significantly reduces the photocatalytic activity.

The amount of loading of cocatalyst CoFe-NP on CdS nanorods was varied and denoted NP-CdS-2, and NP-CdS-3. The detail of the cocatalyst loading is shown in Table S1.

### Synthesis of PBA-CdS

Similarly, CoFe-PBA was loaded on CdS replacing sodium nitroprusside with potassium hexacyanoferrate.

**Table S1.** Description of the catalysts

No.	Catalyst	Amount of CdS	Amount of Co(OAc) <sub>2</sub> ·4H <sub>2</sub> O	Amount of cyanometallate
1	NP-CdS-1	100 mg	10 mg	11 mg Na <sub>2</sub> [Fe(CN) <sub>5</sub> (NO)]
2	NP-CdS-2	50 mg	10 mg	11 mg Na <sub>2</sub> [Fe(CN) <sub>5</sub> (NO)]
3	NP-CdS-3	25 mg	10 mg	11 mg Na <sub>2</sub> [Fe(CN) <sub>5</sub> (NO)]
4	PBA-CdS	50 mg	10 mg	12 mg K <sub>3</sub> [Fe(CN) <sub>6</sub> ]

### **Synthesis of NP-TiO<sub>2</sub>**

CoFe-NP was loaded on TiO<sub>2</sub> following the procedure of NP-CdS-2.

### **Synthesis of NP-g-C<sub>3</sub>N<sub>4</sub>**

CoFe-NP was loaded on g-C<sub>3</sub>N<sub>4</sub> following the procedure of NP-CdS-2.

### **Photocatalytic test**

Photocatalytic hydrogen evolution reactions were carried out in a home-made photocatalytic reactor (30 mL) under the illumination of solar simulator (AM 1.5) with intensity 100 mW cm<sup>-2</sup>. In a typical reaction, the photocatalyst (5 mg) was dispersed in 5 mL aqueous solution of lactic acid (16 % v/v). Further, the reaction mixture was purged with argon to maintain an anaerobic condition. After irradiating the photocatalytic reactor under visible light at room temperature, the gas sample was collected using 1 mL gas tight syringe. The gas sample was then injected in gas chromatograph (SHIMADZU GC-2014, TCD) and the produced H<sub>2</sub> amount was calculated by using calibration curves.

### **Preparation of photoelectrodes**

1 cm x 2 cm FTO glass was washed with water, ethanol and hexane under sonication for 15 minutes and dried at 50 °C for 6 h. 2 mg photocatalyst (CdS, NP-CdS-2 or PBA-CdS) was dispersed in ethanol, and drop cast on FTO (1 cm x 1 cm geometrical surface area). Immediately, 20 μL Nafion solution (ethanolic solution containing 10 μL of Nafion in 1 mL of ethanol) was dropped on the catalyst film as the binder.

### **Photoelectrochemical measurements**

An Autolab workstation (PGSTAT-204) was used to record electrochemical impedance spectra (EIS) and photocurrent-time (*i-t*) data. The photoelectrochemical measurements were carried out in 0.5 M Na<sub>2</sub>SO<sub>4</sub> solution.

The electrochemical cell consisted of a three-electrode system with CdS@FTO, NP-CdS-2@FTO or PBA-CdS@FTO as the working electrode, Pt wire as the counter electrode, and Ag/AgCl as the reference electrode used for the EIS measurements. The EIS spectra were measured at frequencies between 0.001 Hz and 10<sup>5</sup> Hz.<sup>1</sup>

The photocurrent measurements were performed with intermittent visible light using an Xe lamp.

Apparent Quantum Efficiency, AQE (%)

$$= \frac{2 * \text{Number of Hydrogen molecules evolved}}{\text{Number of incident photons}} * 100$$

$$= \frac{2 * n_{H_2,t} * N_A * h * c}{P * S * \lambda_{inc.} * t} * 100$$

$n_{H_2,t}$  = Amount of H<sub>2</sub> evolved (moles)

$N_A$  = Avogadro's Number (6.022 x 10<sup>23</sup> mole<sup>-1</sup>)

$h$  = Planck's Constant (6.626 x 10<sup>-34</sup> m<sup>2</sup> Kg s<sup>-1</sup>)

$c$  = Speed of light (3 x 10<sup>8</sup> ms<sup>-1</sup>)

$P$  = Power Density of incident monochromatic light (Wm<sup>-2</sup>)

$S$  = Irradiation area (m<sup>2</sup>)

$\lambda_{inc.}$  = Wavelength of incident monochromatic light (m)

$t$  = Duration of incident light exposure (s)

At  $\lambda_{inc.} = 400$  nm,

## Figures

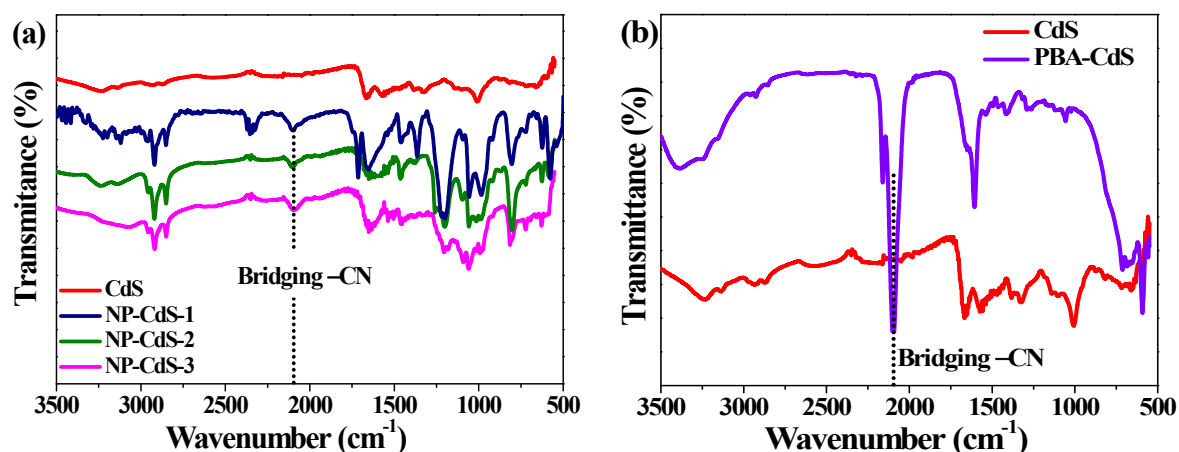


**Figure S1.** (a) FT-IR spectra of CdS, NP-CdS-1, NP-CdS-2 and NP-CdS-3. The NP-CdS showed a peak at  $2107\text{ cm}^{-1}$  corresponding to bridging  $-\text{CN}$  of CoFe-NP;<sup>2</sup> (b) FT-IR spectra of CdS and PBA-CdS. PBA-CdS exhibited a peak at  $2096\text{ cm}^{-1}$  for the bridging  $-\text{CN}$  group.<sup>3,4</sup> The positive shifting of the  $-\text{CN}$  peak in NP-CdS-2 compared to PBA-CdS can be explained by the coordination of stronger  $\pi$ -acceptor ligand  $-\text{NO}$  with Fe center in CoFe-nitroprusside.<sup>5</sup>

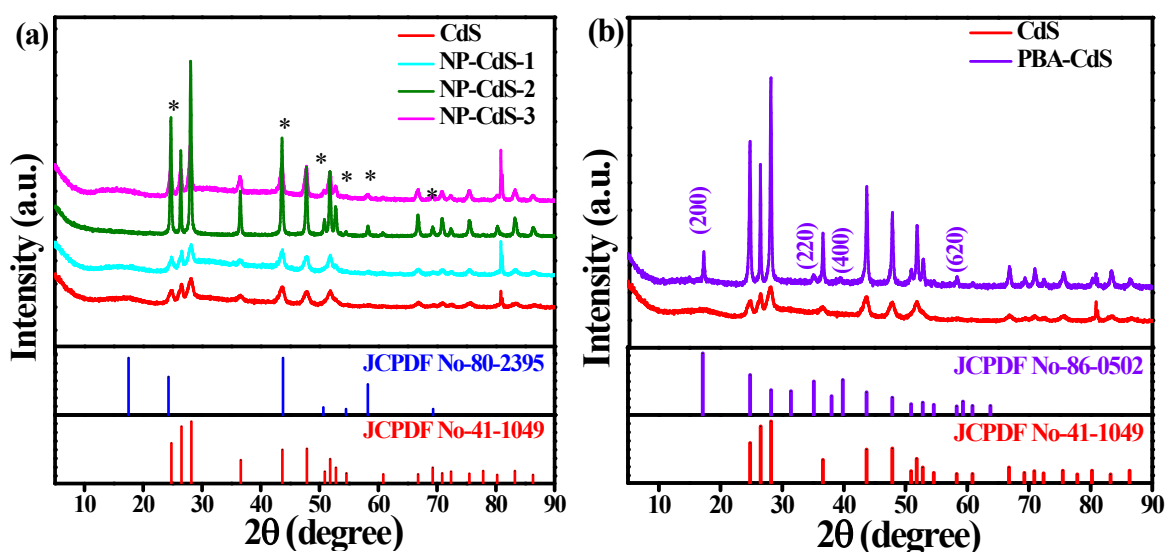


**Figure S2.** (a) The PXRD patterns of CdS, NP-CdS-1, NP-CdS-2 and NP-CdS-3. The peaks are matched with hexagonal phase of CdS (JCPDS No. 41-1049) with space group  $P6_3mc$ .<sup>6</sup> The PXRD peaks of NP-CdS-1, NP-CdS-2 and NP-CdS-3 match well with CdS (JCPDS No. 41-1049) and CoFe-nitroprusside (JCPDS No. 80-2395).<sup>7</sup> The \* marked peaks were assigned for cubic CoFe-nitroprusside with space group  $Fm\bar{3}m$ ; (b) The PXRD pattern of PBA-CdS compared with that of CdS. The \* marked peaks are for CoFe-PBA (JCPDS No. 86-0502) with space group  $Fm\bar{3}m$ .

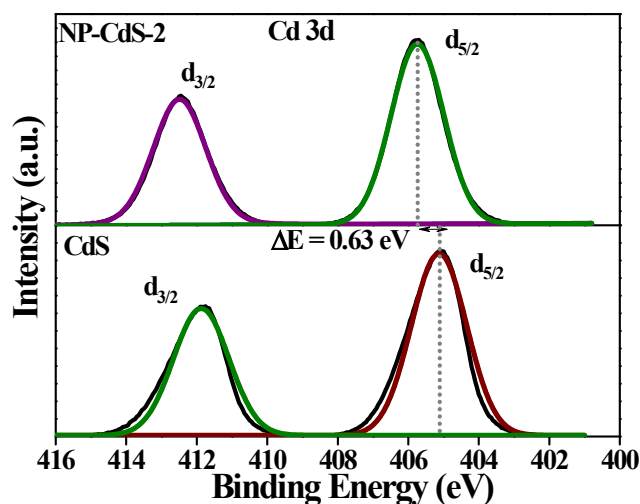


**Figure S3.** The Cd 3d XPS of NP-CdS-2 and CdS. The Cd 3d spectrum of NP-CdS-2 showed two peaks at binding energies 405.74 eV and 412.47 eV for Cd  $3d_{5/2}$  and Cd  $d_{3/2}$ .<sup>8</sup> The peaks corresponding to Cd  $3d_{3/2}$  of NP-CdS-2 showed a positive shift of 0.63 eV compared to that of CdS. The shifting of the binding energy of Cd  $3d_{5/2}$  peak of NP-CdS-2 indicates the charge transfer at the interface of CdS and CoFe-NP through the bridge Cd–CN–Co/Fe.<sup>9</sup> This result also suggests strong electronic interaction between CdS and CoFe-NP.<sup>9</sup>

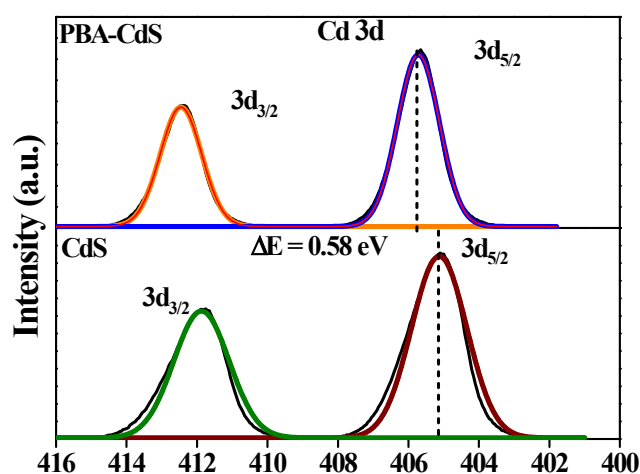


**Figure S3.** The Cd 3d XPS of PBA-CdS and CdS. The Cd 3d spectrum of PBA-CdS showed two peaks at binding energies 405.68 eV and 412.46 eV for Cd  $3d_{5/2}$  and Cd  $d_{3/2}$ , respectively.<sup>8</sup> The peak corresponding to Cd  $3d_{5/2}$  of PBA-CdS showed a positive shift of 0.58 eV as compared to that of CdS. This positive shift in the peaks of  $3d_{5/2}$  and  $3d_{3/2}$  can be explained by the charge transfer from CdS to CoFe-PBA through Cd–CN–Co/Fe bridge.<sup>9</sup>

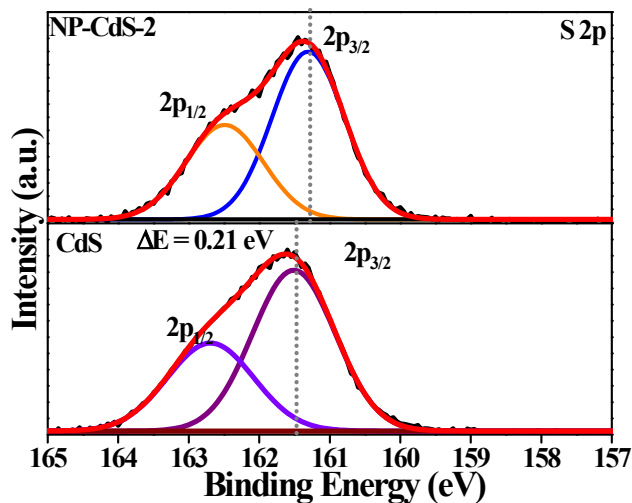


**Figure S4.** The S 2p XPS of NP-CdS-2 and CdS. The S 2p XPS of NP-CdS-2 is fitted into two peaks corresponding to S  $2p_{3/2}$  and S  $2p_{1/2}$ . The peaks corresponding to S  $2p_{3/2}$  in NP-CdS-2 showed a negative shift by 0.21 eV compared to the S  $2p_{3/2}$  of CdS.

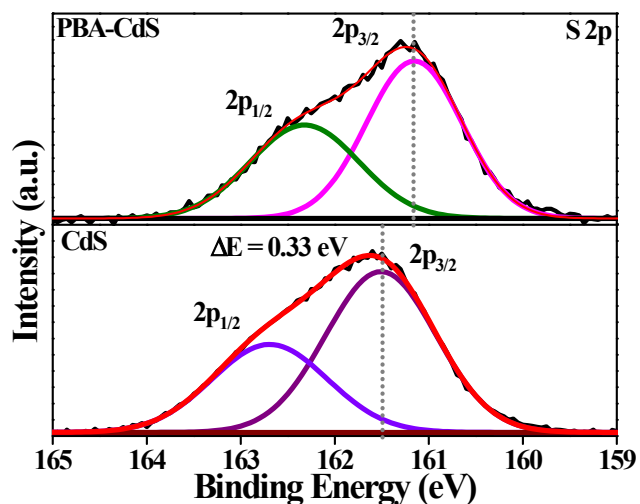


**Figure S4.** The S 2p XPS of PBA-CdS and CdS. The S 2p XPS of PBA-CdS is fitted into two peaks corresponding to S  $2p_{3/2}$  and S  $2p_{1/2}$ . The peaks corresponding to S  $2p_{3/2}$  in PBA-CdS showed a negative shift by 0.33 eV compared to the S  $2p_{3/2}$  of CdS.<sup>8</sup>

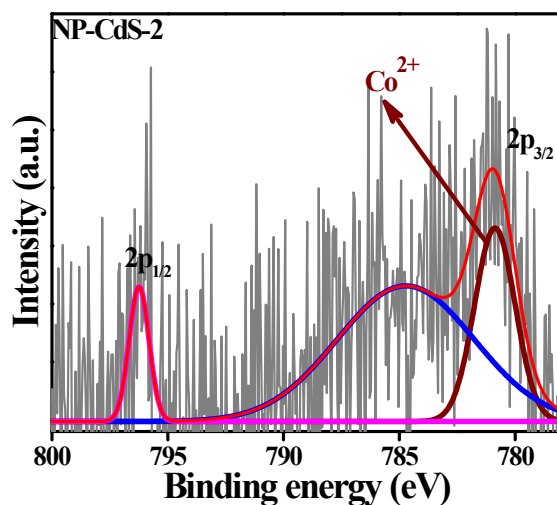


**Figure S5.** Co 2p XPS of NP-CdS-2. The Co 2p of NP-CdS-2 was deconvoluted into two peaks corresponding to the peaks for Co  $2p_{3/2}$  and  $2p_{1/2}$ .<sup>10</sup> The Co  $2p_{3/2}$ - $2p_{1/2}$  spin-orbit coupling spacing  $\sim 16$  eV indicates  $\text{Co}^{2+}$  as the major species.<sup>11</sup> The \* peak at 784.89 eV is attributed to the satellite peak of  $\text{Co}^{2+}$ . The Co  $2p_{3/2}$  spectrum of NP-CdS-2 is showing a negative shifting by 0.35 eV compared to that in CoFe-NP, indicating the modulation of the electronic structure of Co of CoFe-NP after the loading on CdS.<sup>12</sup>

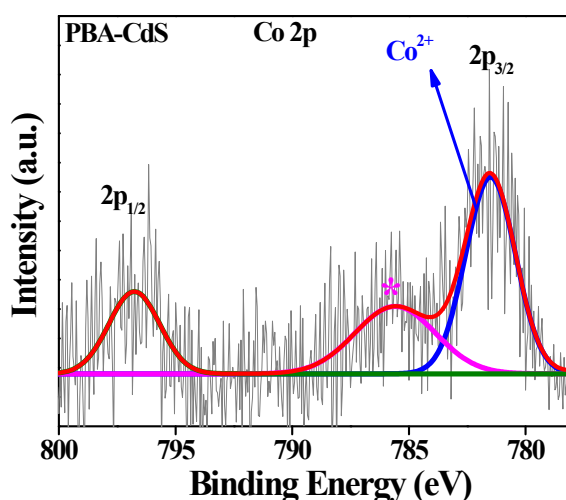


**Figure S6.** Co 2p X-ray photoelectron spectrum of PBA-CdS. The Co 2p XPS of PBA-CdS was deconvoluted into two peaks at the binding energies 781.52 eV and 796.77 eV for Co  $2p_{3/2}$  and  $2p_{1/2}$ , respectively.<sup>13</sup> The Co  $2p_{3/2}$ - $2p_{1/2}$  spin-orbit coupling value was determined to be 15.65 eV, indicating the existence of mixed valent  $\text{Co}^{2+}$  as the major species.<sup>14</sup> The \* peak at 785.58 eV is the satellite peak of  $\text{Co}^{2+}$ .<sup>15</sup>

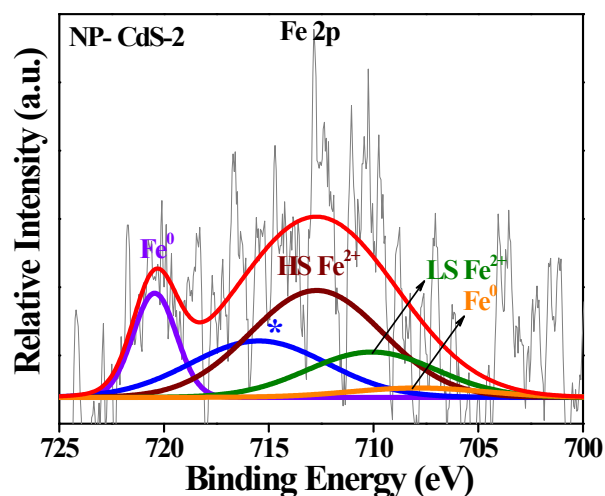


**Figure S7.** Fe 2p XPS of NP-CdS-2 was fitted into the peaks for Fe<sup>0</sup>, high spin (HS) Fe<sup>2+</sup>, and low spin (LS) Fe<sup>2+</sup> and their satellites. The peak at binding energy 707.54 eV belongs to the 2p<sub>3/2</sub> of Fe<sup>0</sup> and the peak at 720.45 eV is attributed to the satellite peak of Fe<sup>0</sup>.<sup>16</sup> The formation of Fe<sup>0</sup> in NP-CdS-2 is due to the reduction of Fe<sup>2+</sup> by the radical CN<sup>•</sup>, formed during the XPS measurements by the loss of -NO.<sup>12</sup> The peak at binding energy 709.74 eV was assigned for low spin Fe<sup>2+</sup>.<sup>12</sup> The peaks at binding energies 710.12 eV and 715.45 eV were fitted for high spin Fe<sup>2+</sup> and its satellite peak (\*), respectively.<sup>12</sup> The Fe 2p<sub>3/2</sub> peak of NP-CdS-2 showed a negative shift of 0.18 eV compared to Fe 2p<sub>3/2</sub> of reported cobalt iron nitroprusside compound, indicating the modulation of the coordination environment around Fe in NP-CdS-2.<sup>12</sup>

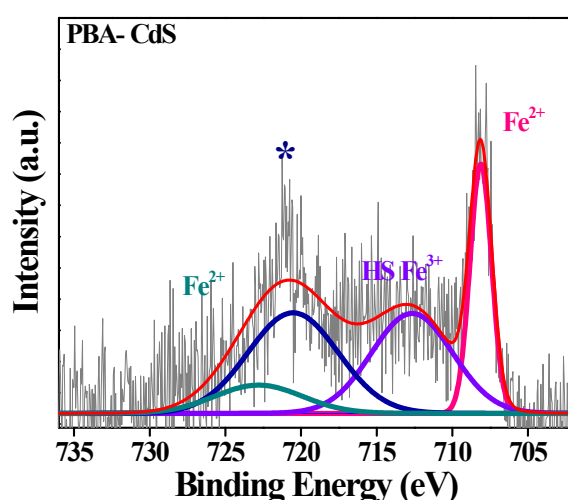


**Figure S8.** The Fe 2p spectrum of PBA-CdS was fitted into four peaks. The peaks at the binding energies 708.05 eV and 720.50 eV were attributed to 2p<sub>3/2</sub> and 2p<sub>1/2</sub> of Fe<sup>2+</sup>.<sup>10</sup> The peaks at binding energies 712.66 eV and 722.7 eV were attributed to 2p<sub>3/2</sub> and 2p<sub>1/2</sub> peaks of high spin Fe<sup>3+</sup>.

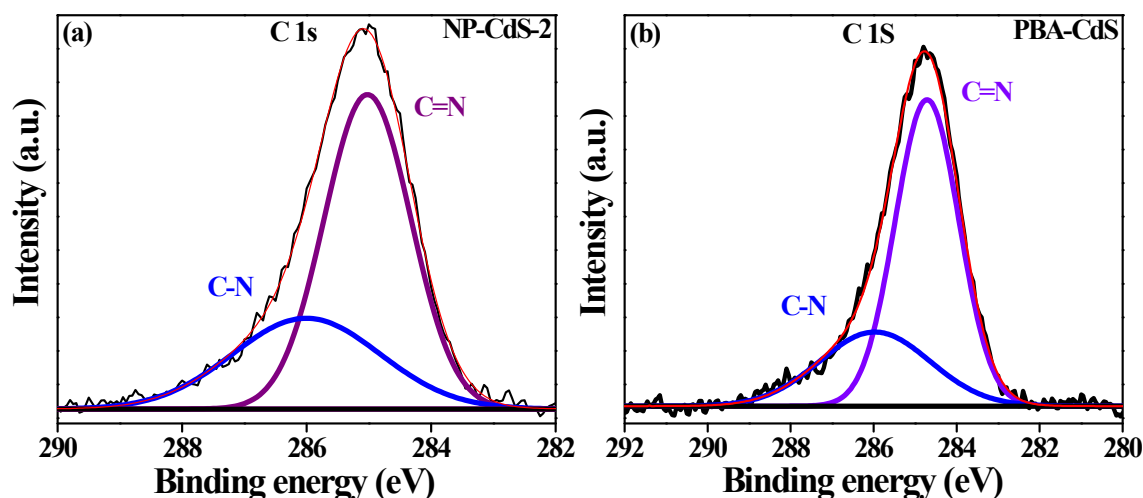


**Figure S9.** (a) C 1s XPS of NP-CdS-2. The C 1s XPS of NP-CdS-2 showed two peaks at binding energies 285.02 eV and 286.01 eV corresponding to C=N, and C-N bonds, respectively from CoFe-NP.<sup>17</sup> (b) C 1s XPS of PBA-CdS showed two peaks at binding energies 284.72 eV and 285.94 eV corresponding to C=C and C-N species, respectively.<sup>18</sup>

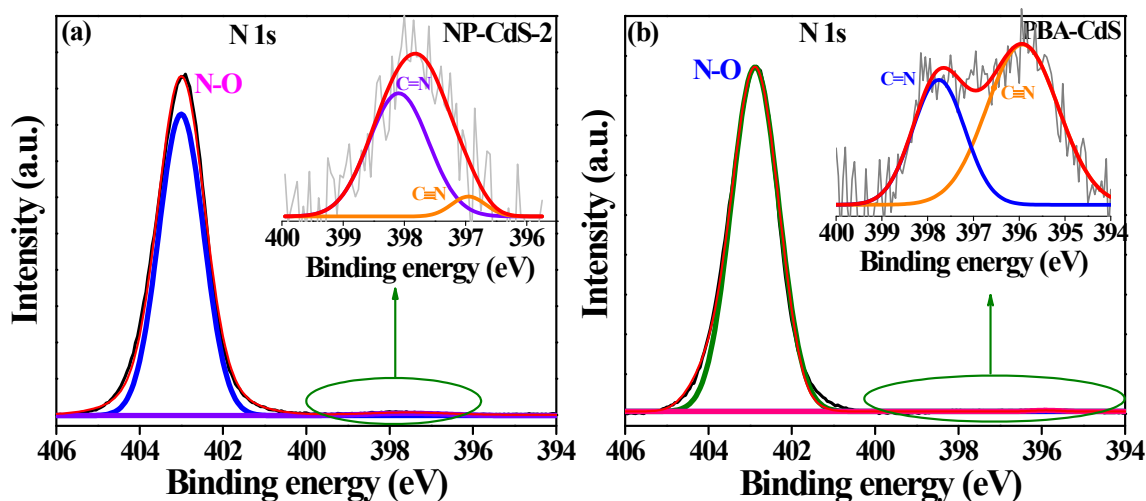


**Figure S10.** (a) The N 1s XP-spectrum of NP-CdS-2 was deconvoluted into three peaks corresponding to the C≡N, C=N, and N-O bonds from CoFe-NP. (b) The N 1s XP-spectrum of PBA-CdS was deconvoluted into three peaks corresponding to the C≡N, C=N, and quaternary N<sup>+</sup>-O<sup>-</sup> bond.<sup>19-21</sup>

**Table S2. Atomic absorption spectroscopy data**

Catalyst	Amount of Co	Amount of Fe
NP-CdS-2	0.45 mg/g	0.24 mg/g
PBA-CdS	5.60 mg/g	11.90 mg/g

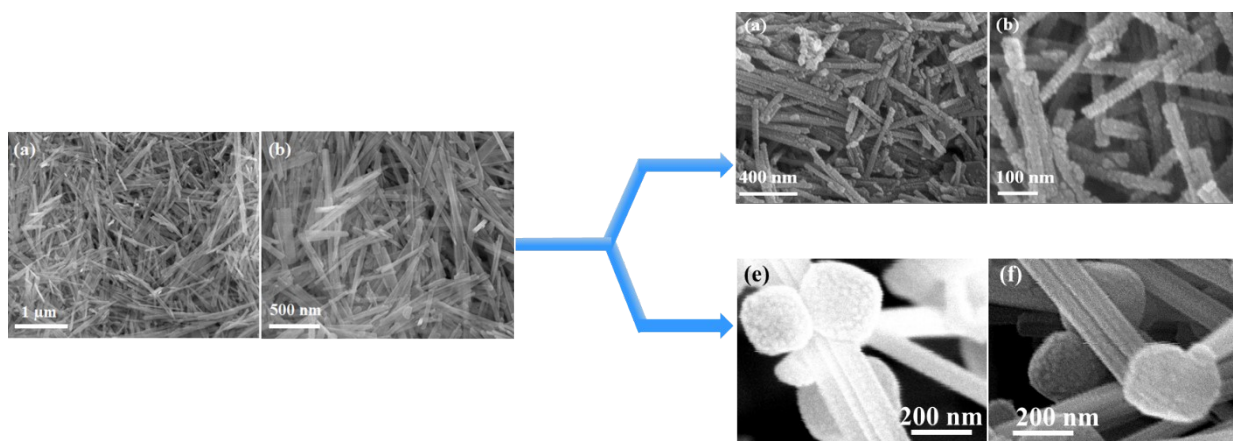


**Figure S11.** (a-b) SEM images of CdS at different resolutions showing nanorod morphology. (c-d) SEM images of NP-CdS-2 at different resolutions showing nanorods with rough surface. (e-f) SEM images of PBA-CdS at different resolutions showing nanorods with beaded structure.

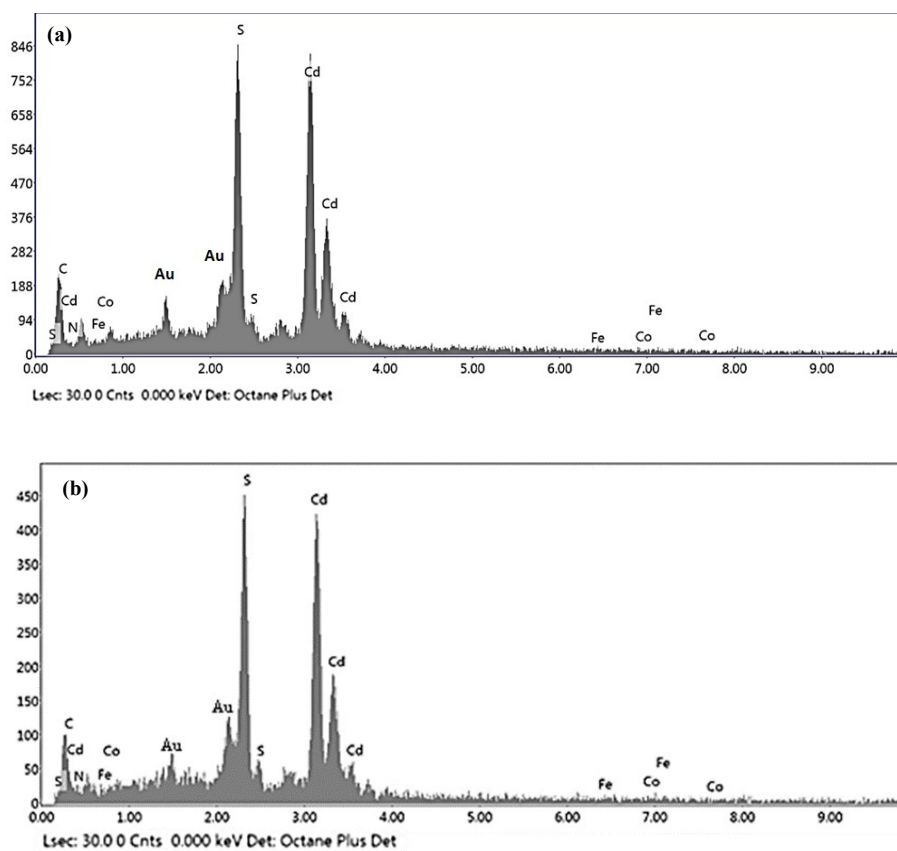


**Figure S12.** (a) Energy dispersive X-ray spectrum of NP-CdS-2 showing the presence of the elements Cd, S, Co, Fe, C, and N. (b) Energy dispersive X-ray spectrum of PBA-CdS showing the presence of the elements Cd, S, Co, Fe, C, and N.

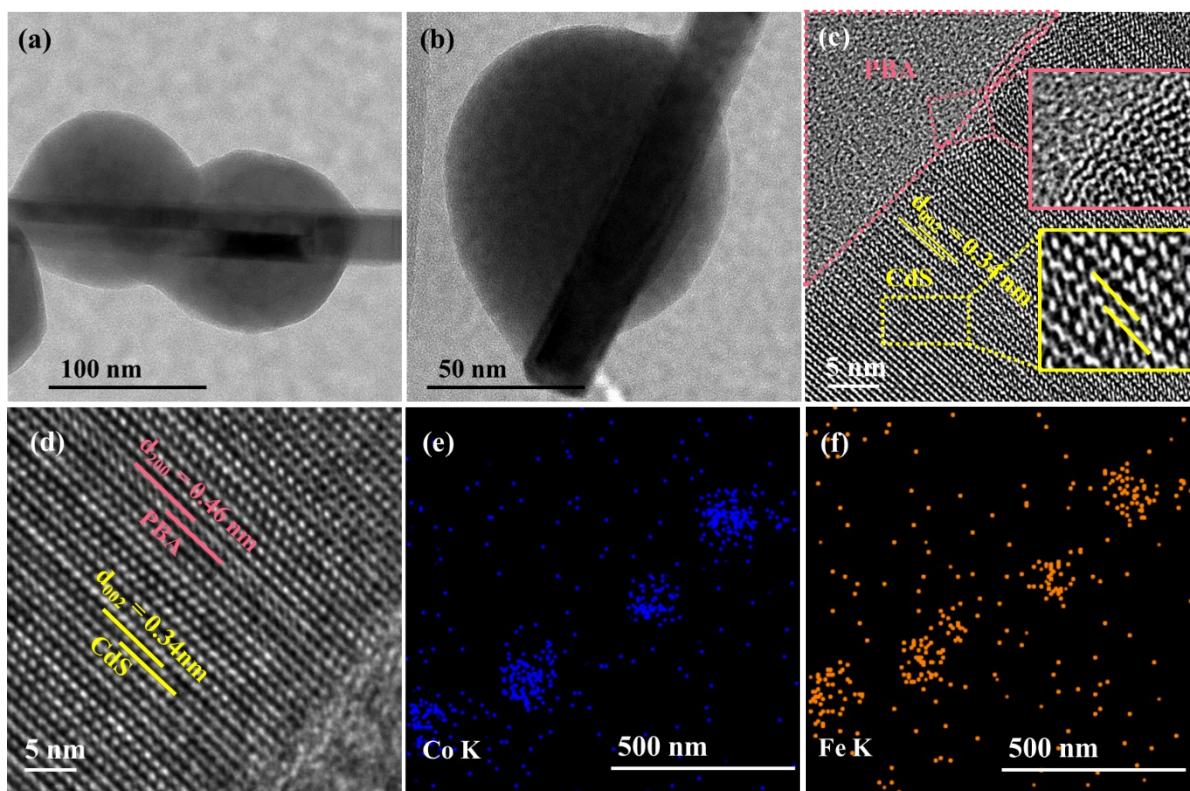


**Figure S13.** (a-b) TEM images of PBA-CdS showing nanorod morphology with bead structure. (c-d) HRTEM of PBA-CdS showing the heterojunction formation between CoFe-PBA and CdS. (e-f) Elemental mapping showing the distribution of Co and Fe.

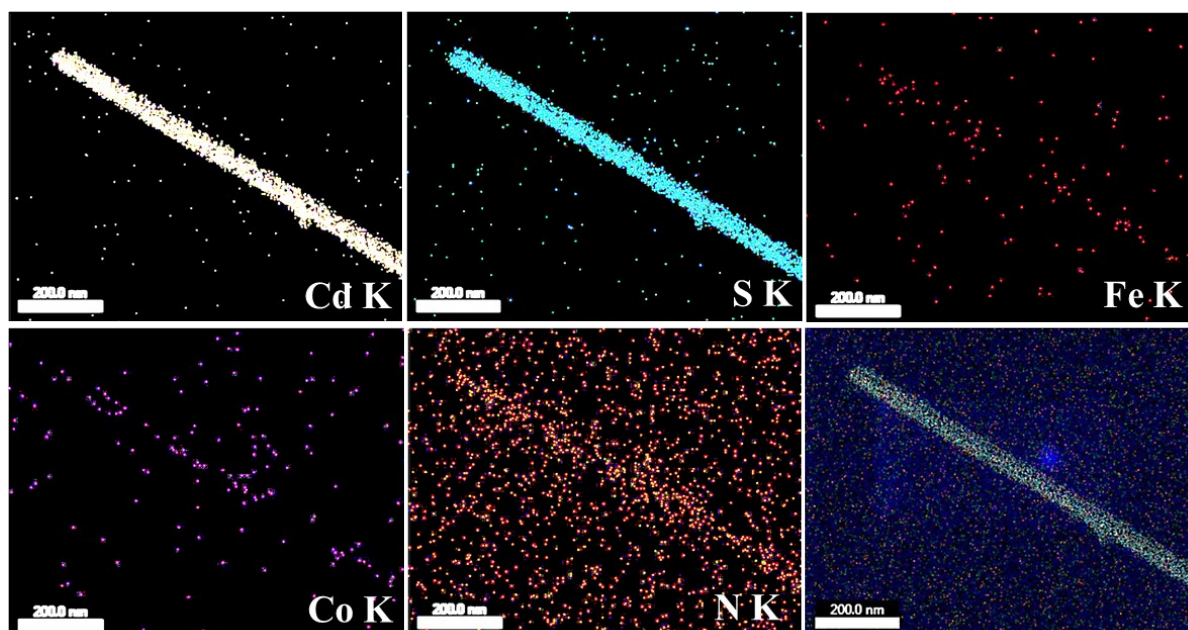


**Figure S14.** EDX elemental mapping of NP-CdS-2 showing the distribution of the elements Cd, S, Co, Fe, C, and N.

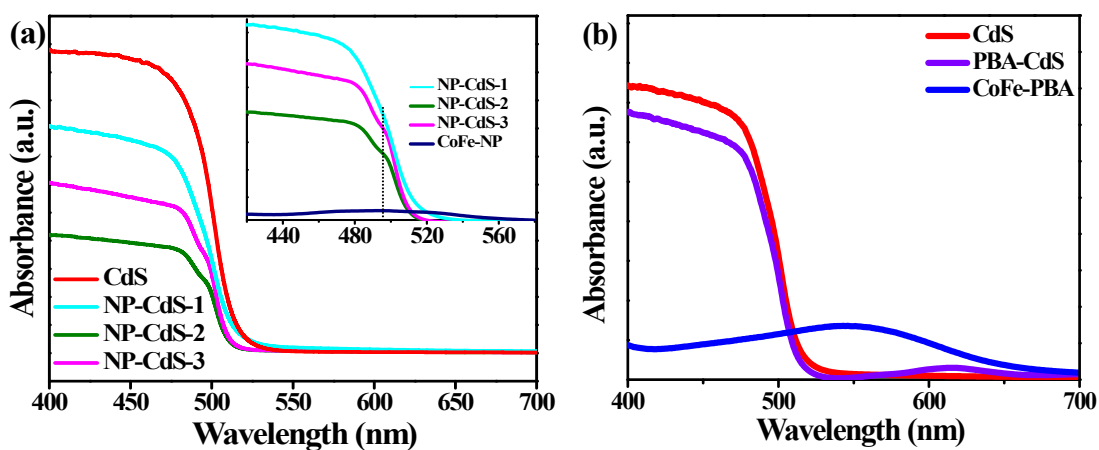


**Figure S15.** (a) The solid-state UV-DRS of CdS, NP-CdS-1, NP-CdS-2, and NP-CdS-3: Inset showing MLCT in CoFe-NP at 497 nm. This absorption corresponding to MLCT appeared as a shoulder in NP-CdS. (b) The solid-state UV-DRS of PBA-CdS compared with CdS. The peak in the region of 550 -650 nm in PBA-CdS arises due to metal to metal charge transfer in CoFe-PBA.<sup>9</sup>

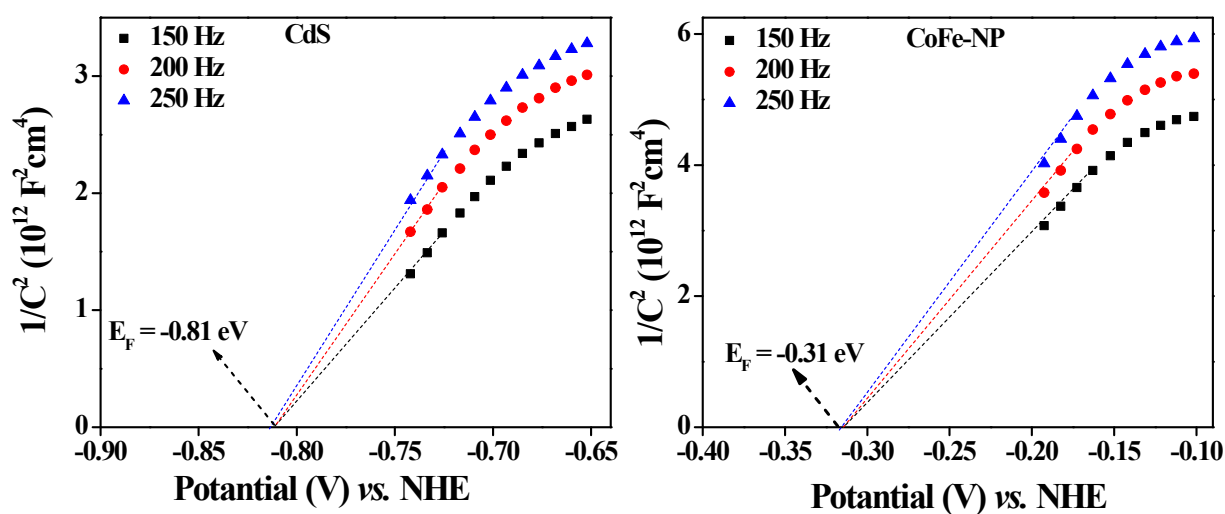


**Figure S16.** Mott-Schottky for CdS and CoFe-NP at frequency 150 Hz, 200 Hz and 250 Hz in 0.5 M Na<sub>2</sub>SO<sub>4</sub> aqueous solution (pH =6.9).

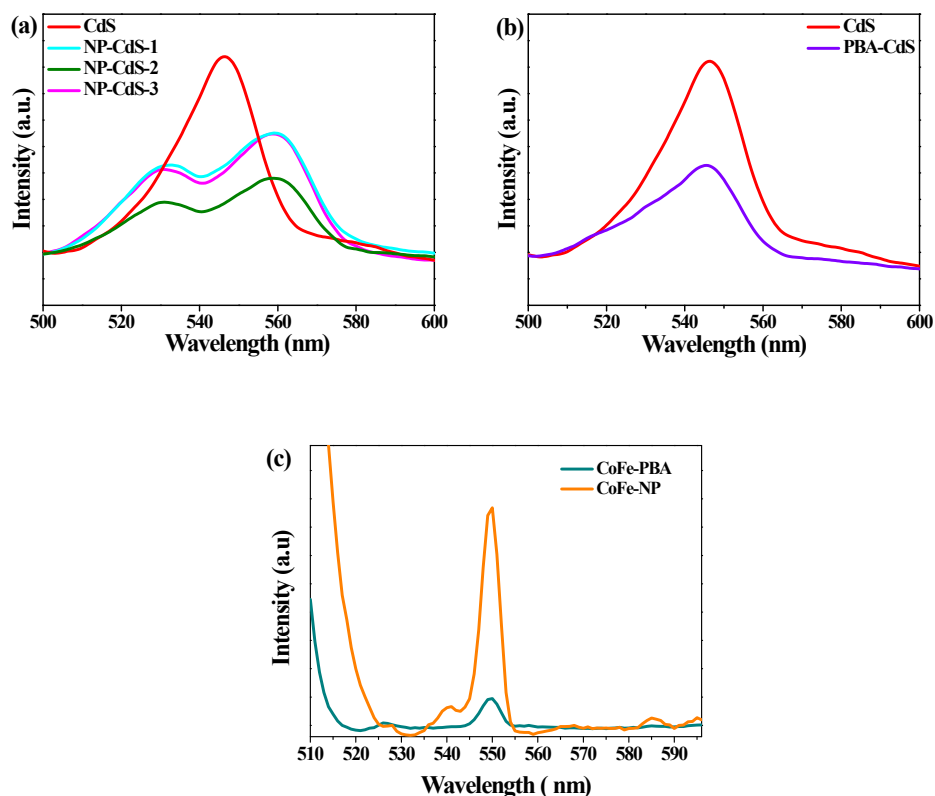


**Figure S17.** (a) Photoluminescence spectra of CdS, NP-CdS-1, NP-CdS-2 and NP-CdS-3. NP-CdS-2 showed a significantly lower PL intensity than pure CdS as well as NP-CdS-1 and NP-CdS-3 because of low charge recombination in NP-CdS-2. PL intensity showed existence of two states in the NP-CdS-2; (b) PL spectra of CdS and PBA-CdS showing lowering of PL intensity after the loading of CoFe-PBA on CdS; (c) PL spectra of CoFe-NP and CoFe-PBA.

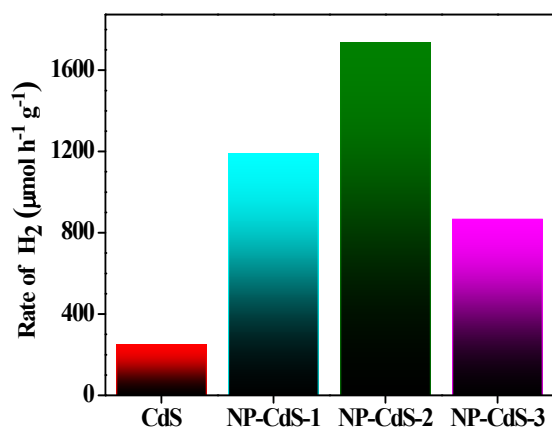


**Figure S18.** The variation in the photocatalytic hydrogen evolution activity attained by the loading of different amount of CoFe-NP on CdS.

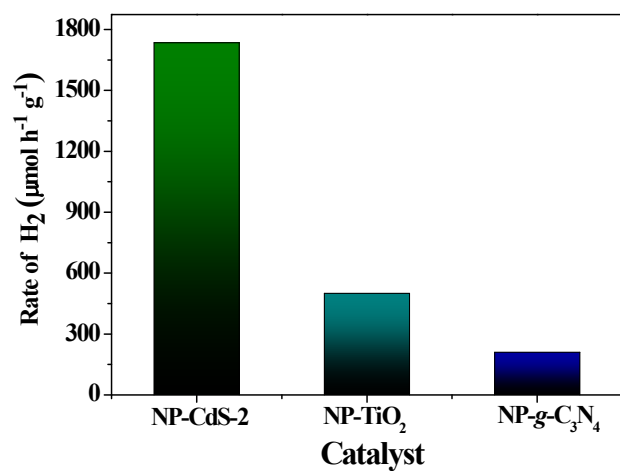


**Figure S19.** The photocatalytic hydrogen evolution activity of NP-CdS-2 compared with NP-TiO<sub>2</sub> and NP-g-C<sub>3</sub>N<sub>4</sub>.

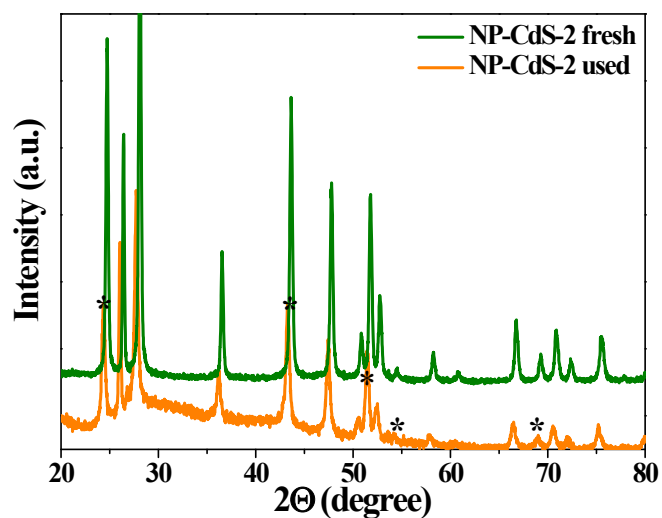


**Figure S20.** The Powder X-ray diffraction pattern of NP-CdS-2 after 24 h photocatalytic HER showed the presence of the peaks of CoFe-NP (\* marked).

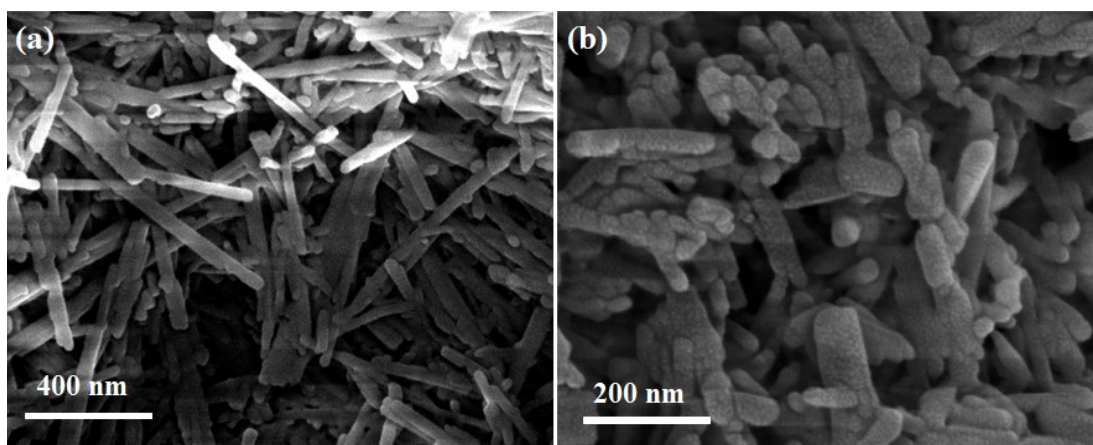


**Figure S21.** (a-b) SEM images of NP-CdS-2 after 24 h photocatalytic HER showing slight agglomeration of nanorods.

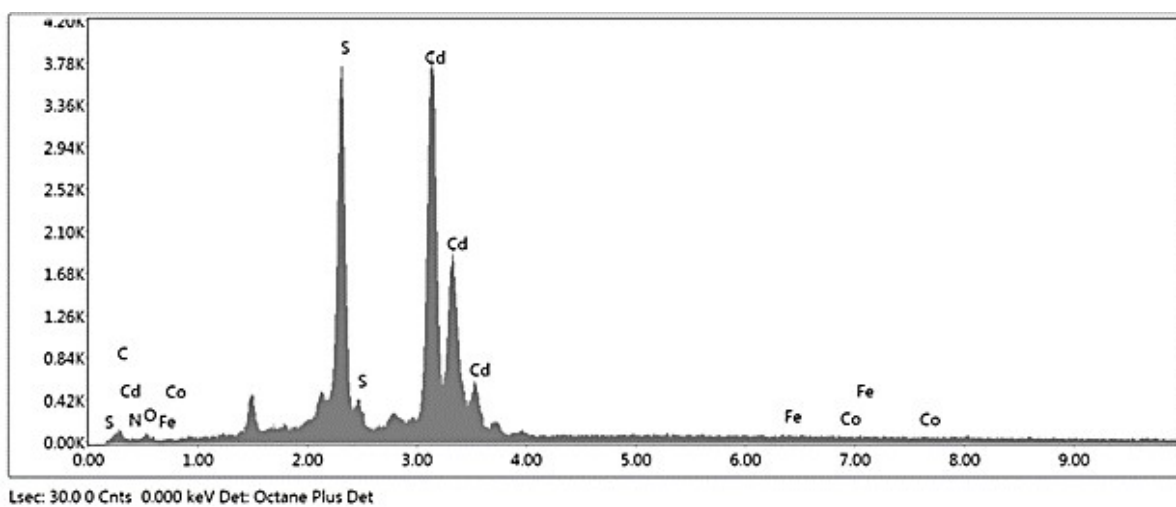


**Figure S22.** Energy dispersive X-ray spectrum of NP-CdS-2 after 24 h photocatalytic HER showing the presence of the elements Cd, S, Co, Fe, C, and N.

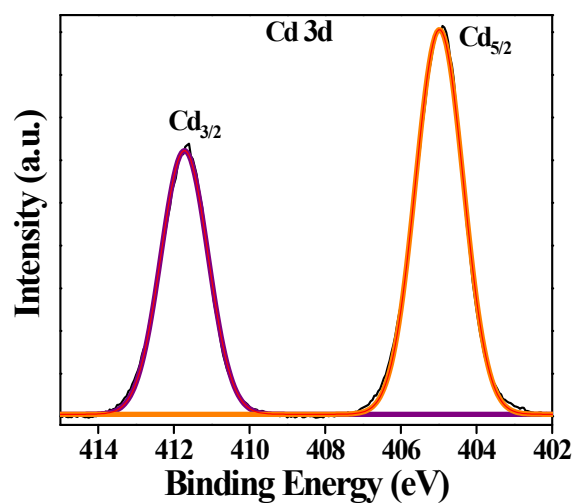


**Figure S23.** The Cd 3d XPS of NP-CdS-2 after 24 h photocatalytic hydrogen evolution. The Cd 3d spectrum of NP-CdS-2 showed two peaks at binding energies 404.96 eV and 411.65 eV for Cd 3d<sub>5/2</sub> and Cd d<sub>3/2</sub>, respectively.<sup>22</sup>

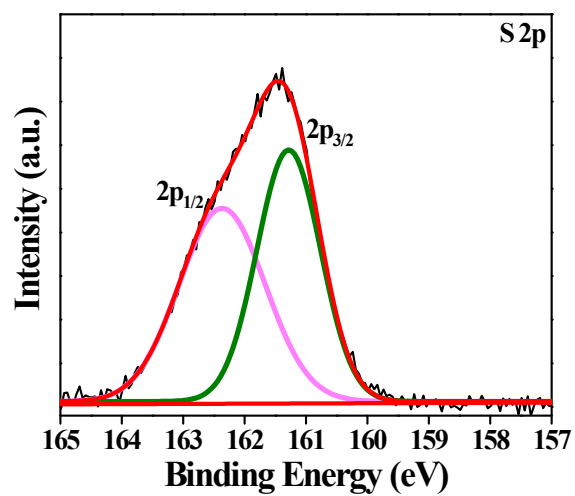


**Figure S24.** The S 2p XPS of NP-CdS-2 after 24 h photocatalytic hydrogen evolution. The S 2p XPS of NP-CdS-2 is fitted into two peaks for 2p<sub>3/2</sub> and 2p<sub>1/2</sub>.<sup>22</sup>

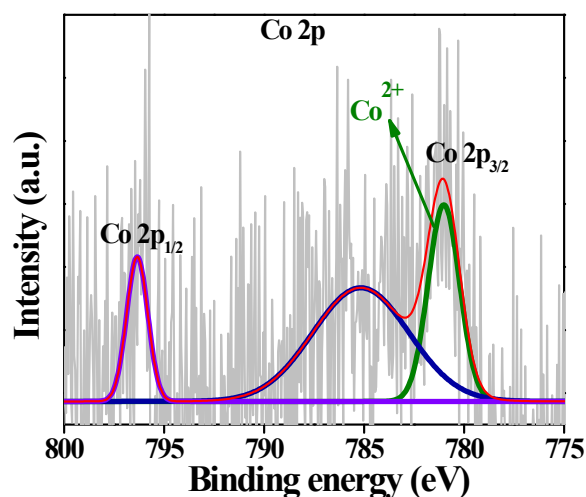


**Figure S25.** Co 2p XPS of NP-CdS-2 after 24 h photocatalytic hydrogen evolution. The Co 2p of NP-CdS-2 was deconvoluted into two peaks corresponding to the Co 2p<sub>3/2</sub> and 2p<sub>1/2</sub>. The 2p<sub>3/2</sub> peaks at binding energies 780.97 eV are assigned to Co<sup>2+</sup> species.<sup>10,11,13</sup>

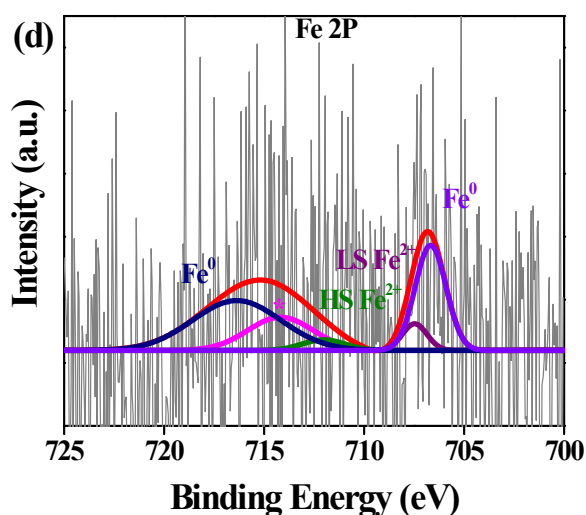


**Figure S26.** Fe 2p XPS of NP-CdS-2 after 24 h photocatalytic hydrogen evolution. The Fe 2p XPS was fitted into the peaks corresponding to Fe<sup>0</sup>, high spin (HS) Fe<sup>2+</sup> and low spin (LS) Fe<sup>2+</sup>. The peaks at binding energy 706.66 eV belongs to the 2p<sub>3/2</sub> of Fe<sup>0</sup> and the peak at 716.45 eV is attributed to the satellite peak of Fe<sup>0</sup>. The peaks at binding energies 711.95 eV and 714.45 corresponding to the high spin Fe<sup>2+</sup> and its satellite peak (\*), respectively.<sup>12,16</sup>

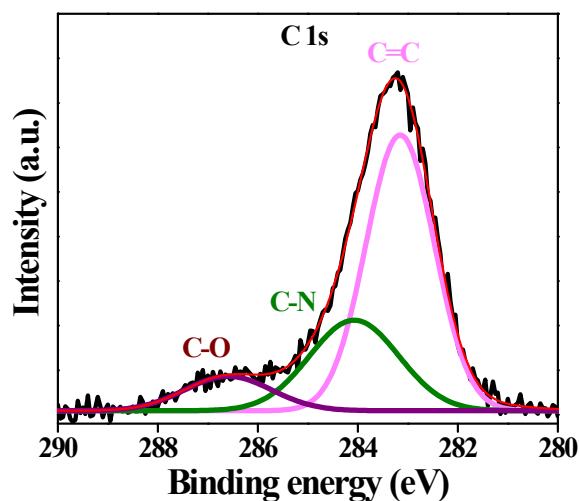


**Figure S27.** C 1s XPS of NP-CdS-2 after 24 h photocatalytic hydrogen evolution showed three peaks at binding energies 283.16 eV 284.09 eV and 286.68 corresponding to C=C, and C–N and C–O bonds from CoFe-NP.<sup>17,18</sup>

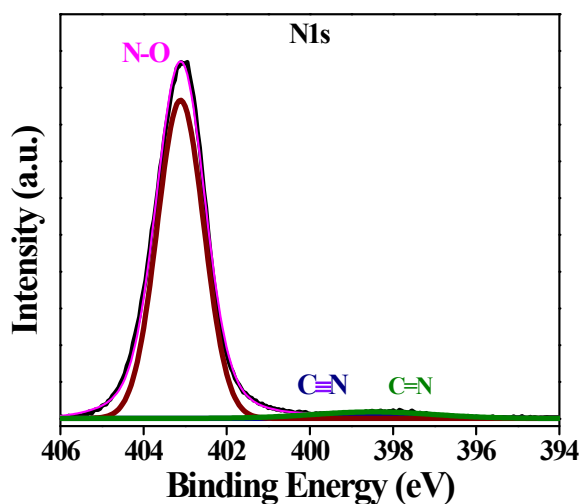


**Figure S28.** N 1s XP-spectrum of NP-CdS-2 after 24 h photocatalytic hydrogen evolution showed three peaks corresponding to the C≡N, C=N, and N–O bonds from CoFe-NP.<sup>19-21</sup>

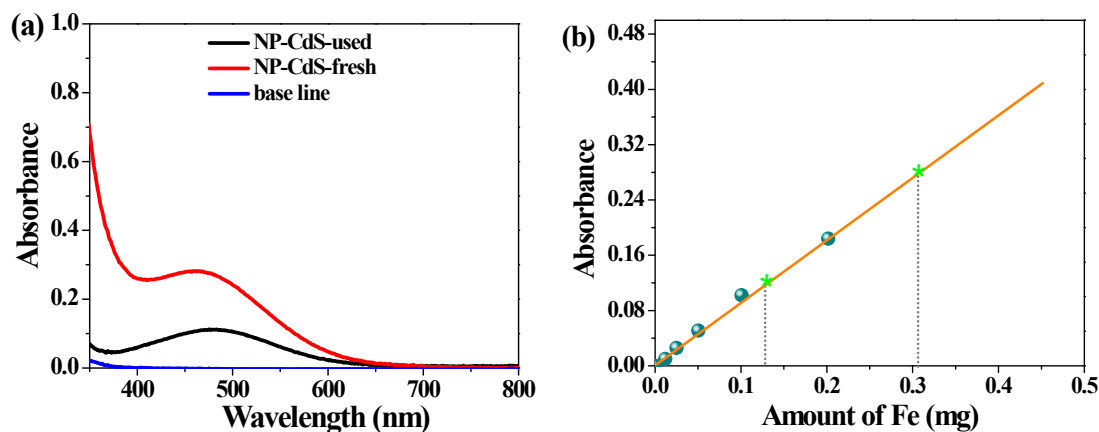


**Figure S29.** (a) UV-vis. spectra for the determination of Fe using thiocyanate method for NP-CdS fresh and used catalyst; (b) Calibration curve for the determination of the amount of Fe in fresh and used catalyst.

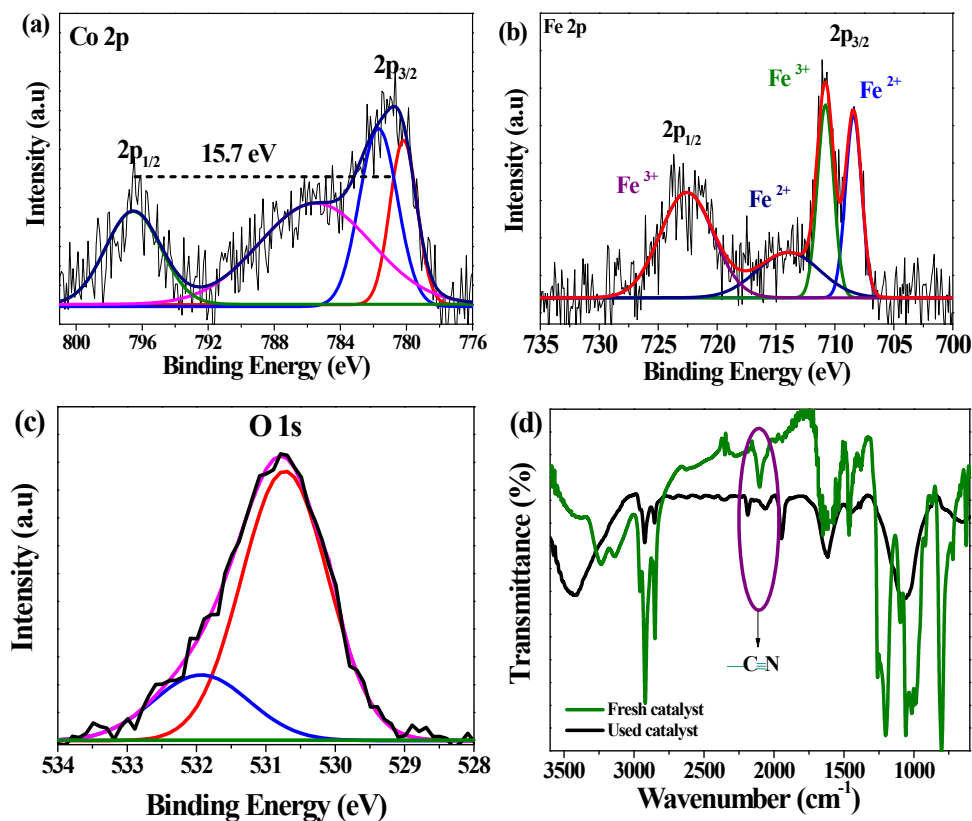


**Figure S30.** XPS and FT-IR of the NP-CdS (5 wt% CoFe-NP) after the photocatalytic HER. (a) The Co 2p XPS of NP-CdS (5 wt%) was deconvoluted into two peaks corresponding to the Co  $2p_{3/2}$  and  $2p_{1/2}$ . The  $2p_{3/2}$  peaks at binding energies 780.17 eV and 781.63 eV are assigned to  $Co^{2+}$  and  $Co^{3+}$  species.<sup>23</sup> (b) Fe 2p XPS of NP-CdS (5 wt%). The Fe 2p XPS was fitted into the peaks corresponding to  $Fe^{2+}$  and  $Fe^{3+}$ .<sup>23</sup> (c) The O 1s XPS was fitted into the peaks corresponding to Co/Fe-O and adsorbed water.<sup>24,25</sup> (d) FT-IR spectra of fresh and used NP-CdS.<sup>2-5</sup>

**Table S3.** Comparison of the photocatalytic activities of CdS-based catalysts

Photocatalyst	Cocatalyst	Sacrificial agent	Light source	Rate of H <sub>2</sub> production (μmol g <sup>-1</sup> h <sup>-1</sup> )	Reference
<b>CdS nanorod</b>	<b>CoFe-NP</b>	<b>Lactic acid</b>	<b>Solar simulator (AM 1.5), 400 W Xe lamp</b>	<b>1735</b>	<b>This work</b>
<b>CdS nanorod</b>	<b>CoFe-PBA</b>	<b>Lactic acid</b>	<b>Solar simulator (AM 1.5), 400 W Xe lamp</b>	<b>1395</b>	<b>This work</b>
<b>CdS nanorod</b>	<b>-</b>	<b>Lactic acid</b>	<b>Solar simulator (AM 1.5), 400 W Xe lamp</b>	<b>250</b>	<b>This work</b>
CdS hollow sphere	ZIF-67	Na <sub>2</sub> S-Na <sub>2</sub> SO <sub>3</sub>	300 W Xe lamp	1721	26
CdS hollow sphere	ZIF-8	Na <sub>2</sub> S-Na <sub>2</sub> SO <sub>3</sub>	300 W Xe lamp	555	26
Flaky CdS	ZIF-67	Lactic acid	5W LED	1232	27
CdS	UiO-66	Lactic acid	300 W Xe lamp	1720	28
CdS nanoparticles	Mo-VC	Lactic acid	300 W Xe lamp	2267	29
CdS/Au-Co	Au	Lactic acid	350 W Xe lamp	1729	30
CdS	Mo <sub>2</sub> N	Lactic acid	300 W Xe lamp	1200	31
CdS nanoparticles	WS <sub>2</sub>	Lactic acid	300 W Xe lamp	1984	32
CdS nanoparticles	MoS <sub>2</sub>	Lactic acid	300 W Xe lamp	1472	[24]
CdS	DETA	H <sub>2</sub> O/ethanol with Triethylamine	300 W Xe lamp	507.37	33

**Table S4.** Exponential curve fitted parameters of transient absorption decay for NP-CdS-2 and CdS.

Catalyst	Wavelength (nm)	$\tau_1$ (ps)	$\tau_2$ (ps)	$\tau_3$ (ps)
CdS	470	$0.8 \pm 0.1$	-	$36.6 \pm 0.7$
	510	$0.4 \pm 0.02$	$12.7 \pm 2.1$	$44.5 \pm 4.9$
NP-CdS-2	470	$0.2 \pm 0.03$	$5.6 \pm 0.4$	$37.9 \pm 1.7$
	510	$0.4 \pm 0.03$	$14.1 \pm 2.3$	$42.6 \pm 7.3$

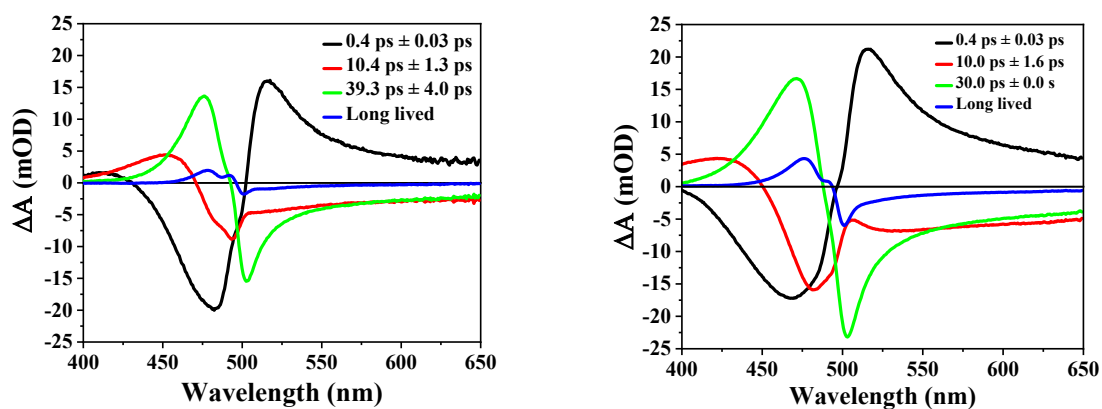


**Figure S31.** Evolution associated decay spectra obtained by global analysis of (a) CdS and (b) NP-CdS-2

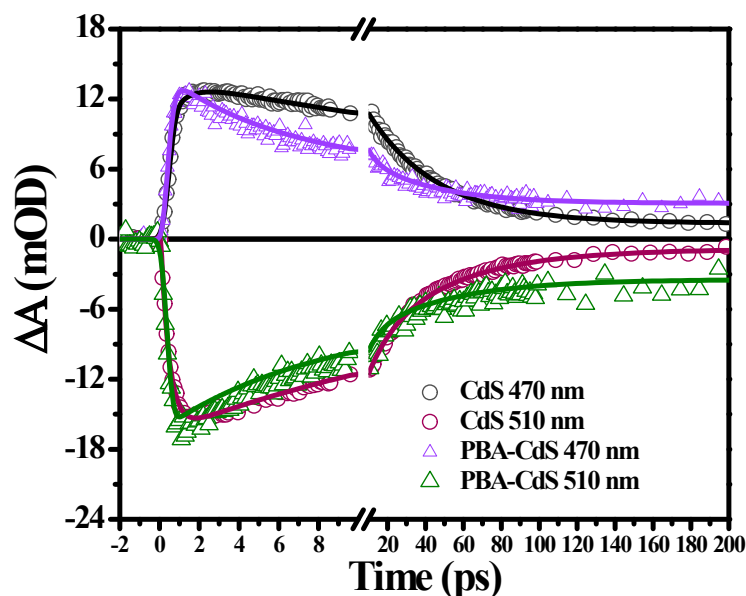


**Figure S32.** Kinetic traces at 470 nm and 510 nm for CdS, NP-CdS-2, and PBA-CdS.

## References

- 1 J. He, L. Chen, F. Wang, Y. Liu, P. Chen, C.-T. Au and S.-F. Yin, *ChemSusChem*, 2016, **9**, 624–630.
- 2 P. Xiong, G. Zeng, L. Zeng and M. Wei, *Dalt. Trans.*, 2015, **44**, 16746–16751.
- 3 X. Lu, H. Xu, T. Yang, X. Chen, Z. Cheng, Q. Hou, X. Lin, S. Liu, S. Wei and Z. Wang, *J. Alloys Compd.*, 2023, **942**, 169004.
- 4 H. Yang, J. Liu, Z. Chen, R. Wang, B. Fei, H. Liu, Y. Guo and R. Wu, *Chem. Eng. J.*, 2021, **420**, 127671.
- 5 L. Reguera, Y. Avila and E. Reguera, *Coord. Chem. Rev.*, 2021, **434**, 213764.
- 6 J. Zhang, S. Z. Qiao, L. Qi and J. Yu, *Phys. Chem. Chem. Phys.*, 2013, **15**, 12088–12094.
- 7 S. Devaramani and P. Malingappa, *Electrochim. Acta*, 2012, **85**, 579–587.
- 8 Q. Zhang, J. Wang, X. Ye, Z. Hui, L. Ye, X. Wang and S. Chen, *ACS Appl. Mater. Interfaces*, 2019, **11**, 46735–46745.
- 9 M. Zhang, Y. Chen, J.-N. Chang, C. Jiang, W.-X. Ji, L.-Y. Li, M. Lu, L.-Z. Dong, S.-L. Li, Y.-P. Cai and Y.-Q. Lan, *JACS Au*, 2021, **1**, 212–220.
- 10 F. Diao, M. Rykær Kraglund, H. Cao, X. Yan, P. Liu, C. Engelbrekt and X. Xiao, *J. Energy Chem.*, 2023, **78**, 476–486.
- 11 T. Ivanova, A. Naumkin, A. Sidorov, I. Eremenko and M. Kiskin, *J. Electron Spectros. Relat. Phenomena*, 2007, **156–158**, 200–203.
- 12 A. Cano, L. Lartundo-Rojas, A. Shchukarev and E. Reguera, *New J. Chem.*, 2019, **43**, 4835–4848.
- 13 P. W. Menezes, A. Indra, V. Gutkin and M. Driess, *Chem. Commun.*, 2017, **53**, 8018–8021.
- 14 P. W. Menezes, A. Indra, D. González-Flores, N. R. Sahraie, I. Zaharieva, M. Schwarze, P. Strasser, H. Dau and M. Driess, *ACS Catal.*, 2015, **5**, 2017–2027.
- 15 G. Ai, Q. Hu, L. Zhang, K. Dai, J. Wang, Z. Xu, Y. Huang, B. Zhang, D. Li, T. Zhang, G. Liu and W. Mao, *ACS Appl. Mater. Interfaces*, 2019, **11**, 33987–33999.
- 16 Y. Liang, P. Liu and G. Yang, *Cryst. Growth Des.*, 2014, **14**, 5847–5855.
- 17 A. L. M. Reddy, A. Srivastava, S. R. Gowda, H. Gullapalli, M. Dubey and P. M.

- Ajayan, *ACS Nano*, 2010, **4**, 6337–6342.
- 18 B. K. Mutuma, C. I. Garcia-Martinez, R. C. Dias, B. J. Matsoso, N. J. Coville and I. A. Hümmelgen, *New J. Chem.*, 2019, **43**, 8418–8427.
- 19 A. A. Ahmad, T. G. Ulusoy Ghobadi, M. Buyuktemiz, E. Ozbay, Y. Dede and F. Karadas, *Inorg. Chem.*, 2022, **61**, 3931–3941.
- 20 M. Zhao, Y. Cao, X. Liu, J. Deng, D. Li and H. Gu, *Nanoscale Res. Lett.*, 2014, **9**, 142.
- 21 N. Fechler, T.-P. Fellinger and M. Antonietti, *J. Mater. Chem. A*, 2013, **1**, 14097–14102.
- 22 Y. Su, D. Ao, H. Liu and Y. Wang, *J. Mater. Chem. A*, 2017, **5**, 8680–8689.
- 23 Y. Lykhach, S. Piccinin, T. Skála, M. Bertram, N. Tsud, O. Brummel, M. Farnesi Camellone, K. Beranová, A. Neitzel, S. Fabris, K. C. Prince, V. Matolín and J. Libuda, *J. Phys. Chem. Lett.*, 2019, **10**, 6129–6136.
- 24 B. Singh and A. Indra, *Dalt. Trans.*, 2021, **50**, 2359–2363.
- 25 A. K. Singh, S. Ji, B. Singh, C. Das, H. Choi, P. W. Menezes and A. Indra, *Mater. Today Chem.*, 2022, **23**, 100668.
- 26 Y. Ke, J. Zhang, L. Liu, X. Li, Q. Liang and Z. Li, *Inorg. Chem.*, 2022, **61**, 10598–10608.
- 27 Z. Jin, Z. Wang, H. Yuan and F. Han, *Int. J. Hydrogen Energy*, 2019, **44**, 19640–19649.
- 28 H.-Q. Xu, S. Yang, X. Ma, J. Huang and H.-L. Jiang, *ACS Catal.*, 2018, **8**, 11615–11621.
- 29 Y. Lei, K. H. Ng, Y. Zhu, Y. Zhang, Z. Li, S. Xu, J. Huang, J. Hu, Z. Chen, W. Cai and Y. Lai, *Chem. Eng. J.*, 2023, **452**, 139325.
- 30 X. Yi, H. Li, P. Wang, J. Fan and H. Yu, *Appl. Surf. Sci.*, 2020, **512**, 144786.
- 31 B. Ma, J. Zhang, K. Lin, D. Li, Y. Liu and X. Yang, *ACS Sustain. Chem. Eng.*, 2019, **7**, 13569–13575.
- 32 J. Chen, X.-J. Wu, L. Yin, B. Li, X. Hong, Z. Fan, B. Chen, C. Xue and H. Zhang, *Angew. Chemie Int. Ed.*, 2015, **54**, 1210–1214.
- 33 W. Zhao, Y. Huang, Y. Liu, L. Cao, F. Zhang, Y. Guo and B. Zhang, *Chem. -A Eur. J.*, 2016, **22**, 15049–15057.